Southern Hemisphere Continental Temperature Responses to Major Volcanic Eruptions Since 1883 in CMIP5 Models

Pamela J Harvey (pamjharvey14@gmail.com)
University of the Witwatersrand https://orcid.org/0000-0002-9559-7561
Stefan W Grab
School of Geography, Archaeology and Environmental Studies, University of the Witwatersrand, Johannesburg, South Africa

Research Article

Keywords: Volcanic Forcing, Southern Hemisphere, CMIP5, Temperature Response, Climate Modelling, Volcanic Eruptions

Posted Date: March 18th, 2021

DOI: https://doi.org/10.21203/rs.3.rs-310211/v1

Version of Record: A version of this preprint was published at Theoretical and Applied Climatology on October 19th, 2021. See the published version at https://doi.org/10.1007/s00704-021-03810-x.

Abstract

Although global and Northern Hemisphere (NH) temperature responses to volcanic forcing have been extensively investigated, knowledge of such responses over Southern Hemisphere (SH) continental regions is still limited. Here we use an ensemble of CMIP5 models to explore SH temperature responses to four major volcanic eruptions: Krakatau (1883), Santa Maria (1902), Agung (1963) and Pinatubo (1991). Focus is on near-surface temperature responses over southern continental landmasses including southern South America (SSA), southern Africa (SAF) and Australia and their seasonal differences. Findings indicate that for all continents, temperature responses were strongest and lasted longest following the Krakatau eruption. Responses in Australia had the shortest lag time, strongest maximum seasonal response, as well as the most significant monthly anomalies. In contrast, SSA records the longest lag time, weakest maximum seasonal temperature response, and lowest number of monthly negative anomalies following these eruptions. In most cases, the strongest single-season response occurred in austral autumn or winter, and the weakest in summer or spring. We tentatively propose that cooler temperature responses are likely caused, at least in part, by the intensification of the westerlies and associated mid-latitude cyclones and anti-cyclones.

1 Introduction

The relationship between volcanoes and climate has long been a scientific fascination (Humphreys 1913; Gilliland 1982; Robock 2000; Allen et al. 2018), and so much so, that Past Global Changes (PAGES) now has a working group examining volcanic impacts on climate and society (VICS). It is well-recognized that volcanic events emitting c. 5Tg or more of sulfur-containing gases into the lower stratosphere, where chemical reactions form sulfate aerosols, can affect climate (Timmreck 2018). These aerosols not only change the earth's energy balance by reducing incoming solar radiation through reflection and scattering, but also cause absorption of near infrared and long-wave radiation, with consequential warming of the lower stratosphere (Stenchikov et al. 1998; Langmann 2014). It is understood that changes in radiation induce stronger zonal winds and increase temperature and density gradients between the poles and equator, thereby strengthening the northern hemisphere (NH) polar vortex (Perlwitz and Graf 1995; Zambri and Robock 2016). However, given the expanse of oceans in mid- to high latitudes of the southern hemisphere (SH), the SH polar vortex and jet streams are more robust. This weakens the expected impact in southerly latitudes (Robock et al. 2007), nonetheless, it too is susceptible to volcanic forcing (Hudson 2012; Kidston et al. 2015).

Major eruptions may cause global annual temperatures to decrease by at least 0.1°C for two to three years following the eruption (Robock 2000; Brönnimann et al. 2019). Findings generally show cooling over much of the NH, particularly in summer, and widespread mid to high latitude winter warming (Stoffel et al. 2015; Zambri and Robock 2016; Zambri et al. 2017). SH temperature responses are somewhat weaker than those in the NH (Man et al. 2014; Raible et al. 2016), with cooling of c. 0.1-0.2°C for 1-2 years after major eruptions (Mass & Portman 1989; Robock & Mao 1995). CMIP5 models have simulated a SH autumn/winter cooling between -0.19°C and -0.36°C (Harvey et al. 2020). Somewhat stronger cooling

responses (< -0.25°C) have been modelled over SH mid-latitudes, but with warming over eastern Antarctica following the Agung (1963), El Chichón (1982) and Pinatubo (1991) eruptions (Ménégoz et al. 2018). Although tropospheric responses to major eruptions still require further detailed investigation, Barnes et al. (2016) have identified stratospheric warming in the tropics and cooling over both poles, following the 1991 Pinatubo eruption. While temperatures cooled over most of South America, strongest negative departures were modelled at higher latitudes following the Pinatubo eruption (Colose et al. 2016). Despite such recent work on volcanic forcing effects on SH climate, a large knowledge gap still remains, with many questions still unanswered. For instance, comparisons of seasonal climatic responses to such eruptions between inter-continental SH landmasses, to our knowledge, has yet to be investigated.

Given that many factors (e.g. eruption season, location and strength; pre-condition of the atmosphere, aerosol altitude) influence climatic response to volcanic forcing (Oman et al. 2005; Colose et al. 2015; Predybaylo et al. 2017; Stevenson et al. 2017; Zuo et al. 2018; Sun et al. 2019, Krishnamohan et al. 2019), responses (spatially and temporally) are likely to differ between eruptions. To this end, our aim is to establish how individual major volcanic eruptions since 1883 may have affected SH continental temperatures, and specifically how these responses varied spatially (within and between continents) and temporally (during specific seasons) following these eruptions. Using historical simulations from the Coupled Model Intercomparison Project, phase 5 (CMIP5) (Taylor et al. 2012), temperature responses following the eruptions of Krakatau (1883), Santa Maria (1902), Agung (1963) and Pinatubo (1991) are investigated.

2 Models And Data

Climate model simulations from the Coupled Model Intercomparison Project, phase 5 (CMIP5) (Taylor et al. 2012), are utilized for the purpose of this study (see Table 1). We use a subset of 11 different models (Table 1), selected based on their ability to simulate a satisfactory temperature response (in Santer et al. 2013; Supplementary Fig. S1) to volcanic forcing in the lower stratosphere (see Barnes et al. 2016 for more details). The first three realizations of each model were used, with the exception of the MIROC-ESM-CHEM model, for which only one realization was available, and the GISS-E2_R model for which two different physics-versions were used. Both physics-version one (p1) and three (p3) were incorporated due to the different ways in which aerosols are calculated (prescribed for p1 and calculated internally in p3). This enabled the analysis of 31 simulations.

For this study, an ensemble of the historical experiments is used, which include both natural (volcanic and solar) and anthropogenic climate forcing and cover the period 1850-2005. Volcanic forcing was not prescribed for CMIP5, so models implemented the forcing from either Sato et al. (1993) or Ammann et al. (2007), except for the MRI-CGCM3 model, which calculated it interactively. Notably, climate models do not perfectly simulate responses to volcanic forcing, and may either over- or under-estimate the response (Neukom et al. 2019). CMIP5 models generally overestimate the response to volcanic forcing (Driscoll et al. 2012; Lehner et al. 2016; Raible et al. 2016). Results thus reflect what the selection of CMIP5 models

show, and may not necessarily accurately represent *actual* near-surface temperature conditions. Results do nevertheless provide valuable indications of *relative* temperature responses to volcanic forcing and offer an opportunity for future comparison with ground-based instrumental records where these exist. We do, however, compare the CMIP5 results with reanalysis data from NOAA/OAR/ESRL, the 20th Century Reanalysis V2 (20CRv2).

Each of the model simulations were linearly regridded to a 2° by 2° lat-long grid before having been combined into a multi-model mean. Near-surface (2m) temperatures are analysed, and all temperatures mentioned in this paper are a SH mean of each continent (calculated from 0° latitude and southwards). For both the CMIP5 and 20CRv2 datasets, annual, seasonal and monthly mean anomalies are presented with respect to a 20-year running mean. So as to calculate statistical significance, a bootstrap approach (Efron 1979) was used to resample the time series of departures 5000 times. To distinguish between random occurrences and significant climatic responses, the 5^{th} and 95^{th} percentiles of the bootstrapped dataset were incorporated to test for significant temperature responses (Haurwitz and Brier 1981; Rao et al. 2017).

Four eruptions from the period 1850-2005 are considered including Krakatau (August 1883), Santa Maria (October 1902), Agung (March 1963) and Pinatubo (June 1991) (Table 2). Apart from Agung (VEI = 4), the selected eruptions had a VEI ≥ 6 and all these are known to have impacted global temperatures, apart from Agung which largely impacted the SH (Mass and Portman 1989; Gleckler et al. 2006; Zanchettin et al. 2012; Khodri et al. 2017; Ménégoz et al. 2018, Harvey et al. 2020). Temperatures are examined for southern South America (SSA) at latitudes 0° to 60°S, southern Africa from 0° to 35°S and Australia which lies between 10°S and 45°S.

3 Results

3.1 Temperature Response to Volcanic Eruptions: Southern South America (SSA)

3.1.1 SSA: Krakatau

Krakatau erupted on 27^{th} August 1883, placing 22Tg of SO_2 into the lower stratosphere (Neely III and Schmidt 2016). In SSA, near-surface temperatures responded significantly (Fig. 1) during all seasons of the first (y1), second (y2) and third (y3) years after the eruption, with austral summer and autumn seasons cooling significantly below normal during the fourth year as well (DJF y1: -0.26°C, y2: -0.26°C, y3 -0.28°C; MAM y1: -0.34°C, y2: -0.26°C, y3: -0.27°C; JJA y1: -0.38°C, y2: -0.42°C, y3: -0.28°C; SON y1: -0.29°C, y2: -0.35°C, y3: -0.28°C) (Fig. 2). The strongest response is measured for the second winter (-0.42°C) and based on a 3-year mean seasonal temperature departure, the strongest responding season was winter (-0.36°C), while the weakest was summer (-0.27°C). The first month in which a significant below-normal anomaly is simulated in SSA is May 1884 (-0.24°C), nine months after the eruption (Fig. 3a). While 78% of monthly anomalies from the time of the event until the end of y3 were below normal, 32% were significantly below normal.

Cooling occurred during all seasons over all of SSA in y1 and y2 (Fig. 4 and Fig. S1, Fig. S2, Fig. S3 in Online Resource 1). Temperatures had recovered over southernmost South America in y3, but remained below normal over the northern regions of SSA during all seasons (apart from autumn when temperatures remained below normal throughout SSA). Winter, which records the most prominent temperature response, had strongest cooling over northern parts of SSA (35-0°S) in y1. In winter of y2, strongest cooling occurred over Chile and western Argentina (between -0.40°C and -0.80°C) over latitudes 40-20°S. However, in y3, temperatures in the southern parts of SSA (60-30°S) had recovered to near normal, while those further north (25°S-0°) remained below normal (between -0.20 and -0.60°C).

3.1.2 SSA: Santa Maria

Santa Maria erupted on 24th October 1902, emitting 3.8Tg of SO_2 into the lower stratosphere (Neely III and Schmidt 2016). Although seasonal temperatures cooled below normal in SSA during the first three years (Fig. 1), responses were only significant in austral autumn, winter and spring of y1 (1903), with the strongest response occurring in autumn (MAM y1: -0.37°C; JJA y1: -0.35°C; SON y1: -0.23°C) (Fig. 2). The strongest 3-year mean seasonal temperature departure was for austral autumn (-0.23°C) and the weakest for austral summer (-0.17°C), and overall considerably weaker than that for Krakatau. From the time of the eruption until the end of y3, none of the negative monthly anomalies were statistically significant, although 87% of monthly temperature anomalies were below normal (Fig. 3a).

Temperatures cooled throughout SSA in both autumn and winter, with northern parts of SSA (30-0°S) experiencing strongest cooling (between -0.20°C and -0.80°C) (Fig. 4, Fig. S2) in y1 (1903). In y2, temperatures in autumn and winter warmed to above normal (between 0.00°C and 0.60°C) over the central regions of SSA (35-20°S), while those in northern and southern regions were below normal (between -0.10°C and -0.60°C). During autumn and winter of y3, temperatures in northern parts of SSA remained below normal (between -0.10°C and -0.60°C), while those in the south returned to near normal (between -0.20°C and +0.20°C). During summer and spring seasons, the response is much weaker (between -0.10°C and -0.40°C), with partial cooling over SSA.

3.1.3 SSA: Agung

Mt Agung erupted on 17th March 1963 and emitted 7.5Tg of SO_2 into the lower stratosphere (Neely III and Schmidt 2016). Only austral winter of 1964 and autumn of 1966 had significant negative temperature departures in SSA (JJA y1: -0.24°C; MAM y3: -0.26°C)(Fig. 2). The greatest single-season response occurred in autumn of y3, and despite this, the strongest 3-year mean seasonal temperature departure was for austral winter (JJA) (-0.19°C), while the weakest was for austral summer (-0.15°C). The first significant monthly temperature departure is noted for January 1964 (-0.27°C), 10 months after the eruption (Fig. 3a). While 91% of monthly temperature anomalies were below normal from the time of the eruption until the end of y3, only 7% were significantly below normal.

Temperatures cooled over portions of SSA during all seasons in y1 (1964) and y2 (Fig. 4 and Fig. S1, Fig. S2, Fig. S3 in Online Resource 1), but it was not until y3 when the entire SSA experienced negative

temperature anomalies. Contrary to the response simulated after the Krakatau and Santa Maria eruptions, temperatures in y2 after the Agung eruption were warmer than normal in northern parts of SSA (between 0.00 and 0.60°C) but remained cooler than normal in southern regions (between -0.10°C and -0.60°C).

3.1. SSA: Pinatubo

Mt Pinatubo erupted on 15th June 1991, emitting 18Tg of SO_2 into the stratosphere (Neely III and Schmidt 2016). Each season exhibited significant mean seasonal responses after the Pinatubo eruption in SSA during y1 (Fig. 1). Austral autumn and winter temperatures responded significantly for one season respectively (y1: -0.32°C, -0.34°C respectively) (Fig. 2). Austral spring and summer experienced significant negative temperature departures for two seasons in y0 and y1 for spring (y0: -0.23°C, y1: -0.24°C), and y1 and y3 for summer (y1: -0.28°C, y3: -0.26°C). While the strongest single-season response occurred in winter, the strongest 3-year mean seasonal temperature departure occurred in austral summer (-0.25°C), and the mean 3-season response for all remaining seasons was -0.21°C. The first month for which a significant anomaly occurred was March 1992 (-0.24°C) (nine months after the eruption) (Fig. 3a). During the period from the eruption date until the end of y3, 81% of monthly anomalies were below normal while 23% were significantly below normal.

Temperatures cooled over all of SSA in y1 during all seasons (Fig. 4 and Fig. S1, Fig. S2, Fig. S3 in Online Resource 1). In y2, temperatures were close to normal for autumn and winter, but summer maintained temperatures below normal (between -0.20°C to -0.80°C) in the central and southernmost regions of SSA, as also found by Colose et al. (2016). Northernmost temperatures remained below normal (between -0.10°C and -0.40°C) during spring of y2. Although temperatures during autumn and winter seemed to recover in y2, they were cooler again in y3 over most of SSA (between -0.10°C and -0.60°C).

3.1.5 SSA Summary

In SSA, significant negative annual temperature anomalies are detected after all major eruptions since 1883. The longest and strongest annual response is measured after Krakatau, which had significant annual anomalies for three years (average of -0.30°C), whereas the annual anomalies following the other three eruptions were only significant for y1 (-0.17°C and -0.22°C respectively). The strongest seasonal response occurred during winter for Krakatau and Pinatubo, and autumn for Santa Maria and Agung, while the weakest response generally occurred during summer. Significant monthly responses typically first occur 9-10 months after an eruption. Spatially, cooling occurred over most of SSA in y1 (except Agung, following which temperatures in the tropics did not fall below normal until y3). Strongest cooling often occurs between 25°S and northwards except after Pinatubo. Temperatures typically first recovered in southern parts of SSA following the investigated eruptions.

3.2 Temperature Response to Volcanic Eruptions: Southern Africa (SAF)

3.2.1 SAF: Krakatau

Following the Krakatau eruption, SAF temperatures were significantly cooler than normal during all seasons in y1 and y2, and in all except autumn in y3 (Fig. 1). The strongest responses appeared in austral autumn and winter during y1 (-0.54°C and -0.53°C respectively). Spring and summer of y1 had anomalies of -0.40°C and -0.35°C respectively. Autumn and winter also displayed the strongest 3-year mean seasonal negative temperature departures of -0.41°C and -0.40°C respectively (Fig. 2), with the weakest 3-season mean occurring in spring (-0.32°C). During the second and third years, mean temperature anomalies ranged between -0.26°C and -0.41°C for all seasons. The first significant monthly temperature response is recorded in February 1884 (-0.34°C), six months after the eruption (Fig. 3b). Between the eruption event and the end of y3, 93% of monthly temperature anomalies were negative, and 39% were significantly below normal.

All of SAF cooled during y1-y3 after the Krakatau eruption. During autumn (Fig. 4), winter (Fig. S2) and spring (Fig. S3) of y1, strong cooling (between -0.40°C and -1.00°C) occurred throughout the sub-continent. The same strong anomalies continued into y2 over southernmost SAF (Namibia, Botswana and South Africa) during summer and autumn, shifting over central SAF during winter but decreasing in spring of y2. In y3, strong cooling (between -0.40°C and -0.80°C) continued over Namibia, Botswana and surrounding regions during summer, and over Namibia and western South Africa during winter and spring (between -0.40°C and -0.60°C).

3.2.2 SAF: Santa Maria

Temperature anomalies following the Santa Maria eruption, although negative for all seasons, were only significant for the summer of y0, autumn and spring of y1, and winter of y2 (-0.28°C, -0.48°C, -0.29°C, -0.32°C respectively)(Fig. 1). Mean winter temperature departures in y1, though not significant, cooled by -0.30°C. The strongest seasonal response occurred in autumn of y1 (-0.48°C), while the most pronounced 3-year mean seasonal temperature departure also occurred in autumn (-0.31°C) and was weakest (-0.21°) during summer (Fig. 2). The first month demonstrating a significant temperature departure is February 1903 (-0.23°C), four months after the eruption (Fig. 3b). While 95% of monthly anomalies from the time of the event until the end of y3 were below normal, only 18% were significantly below normal.

Spatially, all of SAF had below normal temperatures for y1 to y3 during all seasons except spring (Fig. S3) in y3 when temperatures over South Africa and the western coast of SAF remained above normal (between 0.20°C and 0.40°C). Strongest cooling occurred over most of SAF during autumn (Fig. 4) of y1 (-0.40°C to -1.00°C). Notable strong cooling (-0.40°C to -0.60°C) occurred between 20 and 30°S in summer of y1, between 10 and 20°S in winter and spring of y1, and between 15 and 25°S during autumn and winter of y2, which extended to southernmost SAF during spring of y2.

3.2.3 SAF: Agung

Following the Agung eruption, temperature departures were significant for one season only; for autumn (-0.34°C), winter (-0.39°C) and spring (-0.30°C) of y1 and summer of y2 (-0.25°C) (Fig. 1). Although the strongest seasonal response in y1 occurred during winter, the strongest 3-year mean seasonal

temperature departure is measured for summer (-0.23°C), while the weakest 3-season mean departure occurred during spring (-0.19°C) (Fig. 2). Negative temperature anomalies are first significant in September 1963 (-0.22°C), six months after the eruption (Fig. 3b). From the time of the eruption until the end of y3, 82% of monthly temperature anomalies were below normal, however, only 23% were significantly below normal.

All of SAF had negative temperature departures during all seasons in y1 (Fig. 4 and Fig. S1, Fig. S2, Fig. S3 in Online Resource 1). Strong autumn and winter cooling occurred over most of SAF, and over southernmost SAF during spring (between -0.40°C and -0.80°C). All seasonal temperatures, apart from summer, returned to near normal in y2 and y3 (between -0.20°C and 0.20°C), with summer temperatures remaining below normal (between -0.20°C and -0.04°C).

3.2.4 SAF: Pinatubo

SAF temperature anomalies were significantly below normal after the Pinatubo eruption during all seasons of y1, and autumn of y2 (DJF: -0.33°C; MAM y1: -0.35°C; y2: -0.37°C; JJA: -0.35°C; SON: -0.31°C) (Fig. 1). Autumn had the strongest response in y1, and also the strongest 3-year mean seasonal temperature departure (-0.30°C), while the weakest 3-year response occurred in summer (-0.23°C) (Fig. 2). The first month in which a significant temperature departure occurred was February 1992 (-0.28°C), 8 months after the eruption (Fig. 3b). During the period from the eruption date until the end of y3, 91% of monthly anomalies were below normal, of which 28% were significantly below normal.

Throughout y1-y3, all seasonal temperatures cooled to below normal over most of SAF (Fig. 4 and Fig. S1, Fig. S2, Fig. S3 in Online Resource 1). Strong cooling (-0.40°C to -0.60°C) occurred in southernmost regions during summer, autumn and winter of y1, and over the central regions during spring. Strong cooling (-0.40°C to -0.80°C) in y2 only occured during autumn over the central regions (10 to 25°S).

3.2.5 SAF Summary

Mean annual temperatures over southern Africa decreased significantly after all four eruptions in y1, and also in y2 and y3 after Krakatau. The strongest response is detected after Krakatau, and the weakest followed Santa Maria. Seasonal temperature responses are strongest during autumn for most eruptions, apart from Agung, after which winter had the strongest response. The weakest responses occurred in either spring (following Krakatau and Agung) or summer (after Santa Maria and Pinatubo). Significant responses typically occurred 4-8 months after an eruption. Spatially, strongest cooling trends occurred over the central or southern regions of SAF (10°S and southwards).

3.3 Temperature Response to Volcanic Eruptions: Australia

3.3.1 Australia: Krakatau

Following the eruption of Krakatau, temperatures in Australia were significantly cooler than normal during all seasons in y1 (1884) (DJF: -0.38°C; MAM: -0.57°C; JJA: -0.41°C, SON: -0.28°C) (Fig. 1). Significant

anomalies continued into summer of y2 and y3 (y2: -0.31°C; y2: -0.34°C), and winter of y2 (-0.23°C) (Fig. 2). The strongest 3-year mean seasonal departures occurred in autumn (-0.35°C) and weakest in spring (-0.26°C). The first month recording a significant response (-0.31°C) was January 1884 (five months after the eruption) (Fig. 3c). While 95% of monthly anomalies from the time of the event until the end of y3 were below normal, 49% were significantly below normal.

With the exception of spring, cool anomalies occurred over the entire continent during all other seasons in 1884 (Fig. 4 and Fig. S1, Fig. S2, Fig. S3 in Online Resource 1). Strong cooling (-0.40°C to -0.80°C) commences in southern parts of Australia during summer of y1, which expands to the whole continent and intensifies (-0.40°C to -1.20°C) during autumn, but then starts to weaken and spatially retract during winter. However, the cooling effect is still notable in northern regions during winter and spring of y1. Temperature anomalies are weaker in y2, with some being above normal during autumn (0.20°C). Strong cooling (-0.40°C to -0.60°C) occurs again in summer and autumn of y3 over central and eastern Australia.

3.3.2 Australia: Santa Maria

After the Santa Maria eruption, Australian temperature anomalies were below normal during austral autumn and winter of y1 (MAM: -0.31°C; JJA: -0.35°C), spring of y2 (-0.27°C) and winter of y3 (-0.22°C) (Fig. 1). Summer anomalies were not significant, but still cooled by -0.22°C in y1 (Fig. 2). Winter had the strongest modelled response in y1 as well as the strongest 3-year mean seasonal temperature departure (-0.25°C), with summer recording the weakest 3-year mean departure (-0.17°C). Although negative temperature anomalies are modelled for the same month in which Santa Maria erupted, significant cooling (-0.25°C) over Australia is only apparent from the sixth month (April 1903) after the eruption (Fig. 3c). From the time of the eruption until the end of y3, 97% of monthly temperature anomalies were below normal, but only 20% were significantly below normal.

After Santa Maria, cooling occurred over all of Australia during all seasons of y1 (Fig. 4 and Fig. S1, Fig. S2, Fig. S3 in Online Resource 1). Strong cooling (between -0.40°C and -0.60°C) is measured over eastern parts of Australia in autumn and spring, and over western regions in summer and winter of y1. In y2, most of the continent still experienced below normal anomalies, except during summer when temperatures returned to normal over parts of Australia (max 0.20°C). Strong cooling (-0.20 to -0.80°C) only occured over south-western regions during spring. Notable negative temperature departures (-0.40°C to -0.80°C) occurred in eastern regions of Australia, while above normal anomalies (up to 0.40°C) occurred in the western regions during summer of y3.

3.3.3 Australia: Agung

Australian spring temperatures were significantly lower than normal during the same year that Agung erupted (y0: -0.42°C) (Fig. 2). Temperatures then remained significantly below normal during all seasons in y1 (DJF: -0.38°C; MAM: -0.40°C; JJA: -0.40°C; SON: -0.31°C) (Fig. 2). Although the strongest single season response is spring of y0, the strongest 3-year mean seasonal temperature departure occurs in autumn (-0.22°C), and the weakest is modelled for winter (-0.14°C). The first month recording a

significantly below normal temperature was October 1963 (-0.23°C), seven months after the eruption (Fig. 3c). While 80% of monthly temperature anomalies were below normal from the time of the eruption until the end of y3, 34% were significantly below normal.

All of Australia cooled during all seasons in 1964 (Fig. 4 and Fig. S1, Fig. S2, Fig. S3 in Online Resource 1). There were strong negative temperature departures (-0.40°C to -0.80°C) in south-eastern regions throughout all seasons. This strong cooling also occurred throughout the south of Australia in summer, throughout the east of Australia during autumn and most of Australia in winter. Below normal anomalies remained throughout Australia in y2, except in summer when some regions were above normal (max 0.20°C). Temperature anomalies returned to near normal (±0.20°C departures) during all seasons of y3.

3.3.4 Australia: Pinatubo

Significant cooling is measured over Australia after the Pinatubo eruption during spring of y0 (-0.52°C), and autumn (-0.33°C), winter (-0.39°C) and spring (-0.29°C) of y1 (Fig. 1). Although spring of y1 experiences the strongest negative anomaly, the strongest 3-year mean seasonal response occurred in both summer and winter (-0.23°C), and the weakest in both autumn and spring (-0.21°C) (Fig. 2). The first significant negative anomaly is recorded in September 1991 (-0.29°C), three months after the eruption (Fig. 3c). From the time of the eruption until the end of y3, 95% of monthly anomalies were negative, and 40% significantly below normal.

Below normal anomalies occurred throughout Australia during y1-y3 for all seasons except autumn during which temperatures in the west were above normal (between 0.20°C and 0.40°C) in y1 and y2 (Fig. 4 and Fig. S1, Fig. S2, Fig. S3 in Online Resource 1). However, autumn also experienced strong cooling (-0.40°C to -0.80°C) over north-eastern regions in y1. Similar anomalies are modelled for eastern areas of Australia during the summers of y1 and y3, over central and northern areas in winter of y1, and northern areas during spring of y1.

3.3.5 Australia Summary

Mean annual temperatures decreased significantly for one year across Australia following each of the major eruptions investigated, and three years following Krakatau. The strongest (negative) mean annual temperature departures occurred after Krakatau (-0.40°C) and weakest after Santa Maria (-0.28°C). Strongest 3-year negative temperature anomalies were for autumn (after Krakatau and Agung) and winter (after Santa Maria and Pinatubo). The entire continent cooled during all seasons of y1. Near normal or above normal temperatures seem to occur more frequently over Australia than SSA or SAF, but no uniform pattern is apparent.

3.4 CMIP5 comparison to Reanalysis data

The CMIP5 data were compared to the 20CRv2 reanalysis data. We find that most CMIP5 values, both annual and seasonal, are stronger (cooler) than the 20CRv2 values by an average 0.30°C (Table 3). Following the Krakatau eruption, all CMIP5 values are cooler (on average by 0.37°C) than the 20CRv2

values, except during JJA of y1 in SAF and SON of y3 in Australia when the reanalysis temperatures are cooler (by an average of 0.12°C). After the Santa Maria eruption, the CMIP5 annual anomalies are only warmer than the reanalysis data in y2 and y3 in Australia (by -0.03°C and -0.17°C respectively). Seasonal values show that this occurs during DJF, MAM, JJA of y2 and JJA and SON of y3 in Australia but also in SON of y1, and DJF and MAM of y2 in SAF. Modelled CMIP5 anomalies are more often cooler than the 20CRv2 anomalies following the Agung eruption, particularly in SAF in y1 and y2 (annual anomalies by 0.07°C and 0.24°C respectively), and in Australia in y3 (by 0.29°C). This also applies to SSA during JJA and SON of y1 (by 0.29°C and 0.20°C respectively) and MAM of y2 (by 0.17°C). Following Pinatubo, CMIP5 annual anomalies are stronger than the 20CRv2 values in Australia during y1 and y2, in DJF (by 0.09°C and 0.49°C respectively) and SON (by 1.20°C and 0.44°C respectively), but also during JJA in SAF (by 0.01°C and JJA and SON in SAF (by 0.03°C and 0.04°C respectively). There are very few 20CRv2 temperature departures that are significantly below normal following the investigated eruptions. Although no annual anomalies are significantly cooler, SON of y1 following the Pinatubo eruption is significantly cooler over Australia (-1.49°C). In SAF, the only significant temperature anomalies based on the 20CRv2 data occur after the Agung eruption, during MAM of y0 (-0.71°C), and JJA (-0.72°C) and SON (-1.12°C) of y1, while no significantly cool anomalies are recorded over SSA.

4 Discussion

Mean modelled temperature anomalies generally demonstrate that all three continents investigated here experienced strongest departures following the Krakatau eruption. For SAF and Australia, responses were second strongest following the Pinatubo eruption and weakest following Santa Maria. Conversely, in SSA the mean response following Pinatubo was weakest, while the response after Agung was second strongest. Despite the Agung eruption having a strong response in SSA, NH responses following the eruption were minimal (Ménégoz et al. 2018). Conversely, for Santa Maria, NH responses were stronger than those over SSA (Mass and Portman 1989). Following Krakatau, the first three years were significantly cooler for each continent, whereas only y1 was significantly cooler after the eruptions of Santa Maria, Agung and Pinatubo. The shorter-lived response after the later eruptions (Agung and Pinatubo) might, at least in part, be a consequence of increased ocean temperatures associated with enhanced anthropogenic forcing which help regulate surface temperatures (Gleckler et al. 2006).

For all three continents investigated, the number of significant monthly negative temperature anomalies was highest post the Krakatau eruption, second highest following the Pinatubo eruption, and lowest following the Santa Maria eruption. Modelled temperature responses were for the most part weakest for Santa Maria (except in SSA, where the response after Pinatubo was weakest). Such outcomes might be a product of the eruption time (Stevenson et al. 2017; Sun et al. 2019). For example, circulation in the SH is more favourable to aerosol distribution during winter due to strengthening of the Brewer Dobson circulation in both the deep and shallow branches in winter (Perlwitz and Graf 1995; Birner and Bönisch 2010; Young et al. 2011). Agung erupted before austral winter, and Pinatubo during austral winter, allowing for better aerosol distribution soon after the eruptions than Santa Maria, which erupted after the austral winter season when aerosol distribution may have been weaker. Differences in the extent of

climatic response between Pinatubo and Santa Maria might also be due to the height at which aerosols reached the stratosphere. Aerosols from the Pinatubo eruption were likely dispersed at a higher altitude given that the plume reached a considerably higher (c. 40km) altitude than that for Santa Maria (c. 23.7-27km) (Bonadonna and Costa 2013). Recent work by Krishnamohan et al. (2019) advocates that the higher the altitude of aerosol injection, the greater the potential cooling effect, which would support greater cooling associated with Pinatubo than Santa Maria. However, the space-time spread of aerosols may not have as much of an influence in the CMIP5 model outputs.

Notably, strongest and most widespread SH continental negative temperature anomalies following the four major eruptions occur in autumn and to a lesser extent in winter, with exceptions following the Agung and Pinatubo eruptions when Australia experienced strongest responses in spring. In contrast, NH temperatures warm in some regions during boreal winter (Zambri and Robock 2016; Zambri et al. 2017). NH winter warming occurs over mid-high latitudes, and while SH land temperatures do not show warming, there is very little land mass at those SH latitudes. However, Fig. 4 and Fig. S1-S3 show a warming in surface temperatures over the oceans in the mid-high latitudes during all seasons.

Over continental regions of the SH (excluding Antarctica), initial significant negative temperature departures following major volcanic eruptions occur most rapidly (within 5 months on average) over Australia, followed closely by SAF (6-month average), but are somewhat more delayed over SSA (9 months on average). Typically, the first significant response is seen between January and May for SSA, in February in SAF, and between October and April over Australia. Temperature responses following all eruptions except Santa Maria (for which the response was strongest over SAF) are strongest over Australia and weakest over SSA. However, the mean response of all eruptions is equally strong for both SAF and Australia. The overall percentage of months recording significant negative temperature anomalies over the initial three years following major eruptions was highest over Australia (20-49%) and lowest over SSA (0-32%).

Volcanic forcing influences atmospheric circulation even into the stratosphere by affecting stratospheric temperature gradients and wind speed – i.e. the jet streams (Cui et al. 2014; Kidston et al. 2015). Jet streams can affect the Southern Annular Mode (SAM) (Karpechko et al. 2010; Xia et al. 2015), planetary waves, westerly circulation, and storm tracks, and hence influence surface weather (Gallego et al. 2005; Hudson 2012; Kidston et al. 2015). The SH jet stream may seasonally shift by c. 10° (Tyson et al. 2000; Shulmeister et al. 2004; Gallego et al. 2005; Hudson 2012). Although knowledge on how volcanic forcing impacts the jet streams is still limited, it is understood that jet streams were impacted by both the 1982 El Chichón and 1991 Pinatubo eruptions in the NH (Hudson 2012). Hudsons' results indicate that the subtropical jets in both hemispheres initially shifted poleward, and subsequently equatorward, after both eruptions. The study additionally found that the SH Polar jet moved equatorward after the Pinatubo eruption. With mid-latitude circulation being affected by volcanic forcing through major SH circulation variability modes (such as SAM, ENSO, jet streams etc.), it seems that major volcanic eruptions affect mid-latitude cyclones (Picas and Grab 2020). An increased intensity and frequency of cold fronts (associated with mid-latitude cyclones) would unquestionably provide for enhanced cooling over SH

continental regions affected by such frontogenesis (see Grab and Simpson 2000). Topographic differences between the SH continental land masses (i.e. high Andes mountain range along western SSA versus relatively flat relief across western, southern and central Australia) would influence the northerly/easterly spread of such cold air wave disturbances. This may, at least in part, explain why cooling is most enhanced over Australia and least so over much of central SSA, following major eruptions.

Spatially, strongest cooling occurs between 0 and 25°S in SSA (see also Colose et al. 2016), between 20°S and 30°S over SAF, and is highly variable over Australia which is located mostly between 15-35°S. The likely enhanced frequency and/or intensity of mid-latitude cyclones, as discussed above, could consequently enhance cooling over southern to mid-latitude continental regions, particularly during austral autumn-winter-spring. Southwestern Western Australia, southeastern Australia (Smith et al. 1982; Buckley and Leslie 2004) and southern SAF (Tyson et al. 2000) are affected by cyclones/cold fronts under normal conditions, which coincidently are areas of strongest volcanically induced cooling anomalies during austral autumn-winter-spring. Such cold surges in SSA are known to bring frost and freezing temperatures to Brazil, oftentimes damaging crops (Vera and Vigliarolo 2000; Espinoza et al. 2013). The cold surges are also responsible for transporting dryer air northwards, which at times has led to drought, as was the case with the severe 1817 drought over Brazil, soon after the 1815 Tambora eruption (Garreaud 2001).

The comparison between the CMIP5 data outputs and the 20CRv2 reanalysis data suggests that the CMIP5 models have overestimated the cooling response to volcanic eruptions over SH continental regions of SSA, SAF and Australia. The fact that CMIP5 overestimates the response to volcanic forcing has also been noted by Driscoll et al. (2012), Marotzke and Forster (2015) and Chylek et al. (2020). However, the 20CRv2 outputs are themselves not an absolutely accurate. While the reanalysis data has successfully captured most SH atmospheric circulation during the period of 1979 to 2010, data pre 1979 has greater discrepancies due to the lack of available observational data (Ke and Hui 2013; Zhang et al. 2013b). This means that the data covering the period of the Pinatubo eruption is more accurate, but that inaccuracies likely exist for temperatures following the eruptions of Krakatau, Santa Maria and Agung. While the CMIP5 models have been said to inaccurately represent SH circulation responses to volcanic forcing, McGraw et al. (2016) argues that the observations do fall within the distributions of modelled SH circulation, in particular the Southern Annular Mode, and Barnes et al. (2016) suggests that the internal climate variability may cause the response to volcanic eruptions seen in the CMIP5 models, to be disguised in the observed response. This leaves a lot of opportunity for CMIP6 to improve the modelled response to volcanic forcing.

5 Conclusion

Until recently, little attention has been given to volcanic forcing impacts on climates of the SH, with a general perception that such forcing has had relatively minimal impact on the SH in relation to its northern counterpart. Attention is here given to the SH with a case of examining such forcing at finer

spatial and temporal resolutions than earlier approaches (i.e. at continental rather than hemispheric scale and seasonal rather than annual scale). Investigations at such a finer scale are able to demonstrate, for the first time, that (significant) negative temperature departures over SH land masses typically occur first over parts of Australia and lag most strongly over SSA. In addition, strongest cooling is noticed over parts of Australia and weakest responses measured over SSA. Strongest responses generally occur during austral autumn, and are usually weakest during spring. We postulate that cooling anomalies during austral autumn and winter in particular, are associated with an increased intensity and/or frequency of mid-latitude cyclones passing over southern continental land masses. Such increased intensity of mid-latitude cyclones is likely caused by the intensification of the westerly winds associated with a positive SAM phase simulated in CMIP5 models. However, other SH circulation variability modes such as ENSO are also likely contributing factors that would require further investigation and verification. Given the many climate sensitive socio-economic systems in southerly regions of SH land masses, it would be beneficial to model such volcano-climate forcing at finer spatial and temporal scales, in order to have a better predictive sense of likely future climate responses to any future major eruptions in order to allow for appropriate preparation for such scenarios.

Abbreviations

Southern South America: SSA

Southern Africa: SAF

y0= Year of the eruption

y1= 1st calendar year after the eruption

y2= 2nd calendar year after the eruption

y3=3rd calendar year after the eruption

Declarations

Funding:

National Research Foundation (NRF): Pamela J. Harvey. Grant: 102161

National Research Foundation (NRF): Pamela J. Harvey. Grant: 111491

Conflicts of interest/Competing interests:

None

Availability of data and material:

CMIP5 data are available via the Earth System Grid Federation (ESGF) portal https://esgf-data.dkrz.de/projects/esgf-dkrz/

CR20v2 data are available from the NOAA/OAR/ESRL PSL https://psl.noaa.gov/data/gridded/data.20thC_ReanV2.html

Code availability:

Not applicable

Authors' contributions:

PJH conducted the data analyses and wrote the initial manuscript, SWG edited the manuscript. Both authors reviewed the final manuscript.

Ethics approval:

Not applicable

Consent to participate:

Not applicable

Consent for publication:

Not applicable

Acknowledgments

We thank the World Climate Research Programme's Working Group on Coupled Modelling that made CMIP5 what it is today. We thank all modelling groups (listed in Table 1) that contributed to CMIP5 and made their model outputs available. Data are available at: https://esgf-data.dkrz.de. We thank the NOAA/OAR/ESRL PSL, Boulder, Colorado, USA for providing the 20th Century Reanalysis V2 (CR20v2) data which was obtained from https://psl.noaa.gov/data/gridded/data.20thC_ReanV2.html. We also thank the National Research Foundation (NRF) for funding this research.

References

1. Allen KJ, Cook ER, Evans R, et al (2018) Lack of cool, not warm, extremes distinguishes late 20th Century climate in 979-year Tasmanian summer temperature reconstruction. Environ Res Lett 13:034041. https://doi.org/10.1088/1748-9326/aaafd7
2. Ammann CM, Joos F, Schimel DS, et al (2007) Solar influence on climate during the past millennium: Results from transient simulations with the NCAR Climate System Model. Proc Natl Acad Sci 104:3713–3718. https://doi.org/10.1073/pnas.0605064103

3. Barnes EA, Solomon S, Polvani LM (2016) Robust wind and precipitation responses to the Mount Pinatubo eruption, as simulated in the CMIP5 models. J Clim 29:4763–4778. https://doi.org/10.1175/JCLI-D-15-0658.1
4. Birner T, Bönisch H (2010) Residual circulation trajectories and transit times into the extratropical lowermost stratosphere. Atmospheric Chem Phys Discuss 10:16837–16860. https://doi.org/10.5194/acpd-10-16837-2010
5. Bonadonna C, Costa A (2013) Plume height, volume, and classification of explosive volcanic eruptions based on the Weibull function. Bull Volcanol 75:742. https://doi.org/10.1007/s00445-013-0742-1
6. Brönnimann S, Franke J, Nussbaumer SU, et al (2019) Last phase of the Little Ice Age forced by volcanic eruptions. Nat Geosci. https://doi.org/10.1038/s41561-019-0402-y
7. Buckley BW, Leslie LM (2004) Preliminary climatology and improved modelling of south Indian Ocean and Southern Ocean mid-latitude cyclones. Int J Climatol 24:1211–1230. https://doi.org/10.1002/joc.1050
8. Chylek P, Folland C, Klett JD, Dubey MK (2020) CMIP5 climate models overestimate cooling by volcanic aerosols. Geophys Res Lett 47:. https://doi.org/10.1029/2020GL087047
9. Colose CM, LeGrande AN, Vuille M (2015) The influence of tropical volcanic eruptions on the climate of South America during the last millennium. Clim Past 11:3375–3424. https://doi.org/10.5194/cpd-11-3375-2015
10. Colose CM, LeGrande AN, Vuille M (2016) The influence of volcanic eruptions on the climate of tropical South America during the last millennium in an isotope-enabled general circulation model. Clim Past 12:961–979. https://doi.org/10.5194/cp-12-961-2016
11. Cui X, Gao Y, Sun J (2014) The response of the East Asian summer monsoon to strong tropical volcanic eruptions. Adv Atmospheric Sci 31:1245–1255. https://doi.org/10.1007/s00376-014-3239-8
12. Dogar MM, Stenchikov G, Osipov S, et al (2017) Sensitivity of the regional climate in the Middle East and North Africa to volcanic perturbations: sensitivity of MENA region to volcanism. J Geophys Res Atmospheres 122:7922–7948. https://doi.org/10.1002/2017JD026783
13. Driscoll S, Bozzo A, Gray LJ, et al (2012) Coupled Model Intercomparison Project 5 (CMIP5) simulations of climate following volcanic eruptions. J Geophys Res Atmospheres 117:D17105. https://doi.org/10.1029/2012JD017607
14. Efron B (1979) Bootstrap Methods: another look at the Jackknife. Ann Stat 7:1–26. https://doi.org/10.1214/aos/1176344552
15. Esper J, Schneider L, Krusic PJ, et al (2013) European summer temperature response to annually dated volcanic eruptions over the past nine centuries. Bull Volcanol 75:736. https://doi.org/10.1007/s00445-013-0736-z
16. Espinoza JC, Ronchail J, Lengaigne M, et al (2013) Revisiting wintertime cold air intrusions at the east of the Andes: propagating features from subtropical Argentina to Peruvian Amazon and

relationship with large-scale circulation patterns. Clim Dyn 41:1983–2002. https://doi.org/10.1007/s00382-012-1639-y

17. Gallego D, Ribera P, Garcia-Herrera R, et al (2005) A new look for the Southern Hemisphere jet stream. Clim Dyn 24:607–621. https://doi.org/10.1007/s00382-005-0006-7
18. Garreaud RD (2001) Subtropical cold surges: regional aspects and global distribution. Int J Climatol 21:1181–1197. https://doi.org/10.1002/joc.687
19. Gilliland RL (1982) Solar, volcanic, and CO2 forcing of recent climatic changes. Clim Change 4:111–131. https://doi.org/10.1007/BF02423387
20. Gleckler PJ, Wigley TML, Santer BD, et al (2006) Volcanoes and climate: Krakatoa's signature persists in the ocean. Nature 439:675. https://doi.org/10.1038/439675a
21. Grab SW, Simpson AJ (2000) Climatic and environmental impacts of cold fronts over KwaZulu-Natal and the adjacent interior of southern Africa. South Afr J Sci 96:602–608
22. Harvey PJ, Grab SW, Malherbe J (2020) Major volcanic eruptions and their impacts on southern hemisphere temperatures during the late 19th and 20th centuries, as simulated by CMIP5 models. Geophys Res Lett 47:. https://doi.org/10.1029/2020GL087792
23. Haurwitz MW, Brier GW (1981) A critique of the Superposed Epoch Analysis Method: Its application to solar–weather relations. Mon Weather Rev 109:2074–2079. https://doi.org/10.1175/1520-0493(1981)109<2074:ACOTSE>2.0.CO;2
24. Hudson RD (2012) Measurements of the movement of the jet streams at mid-latitudes, in the Northern and Southern Hemispheres, 1979 to 2010. Atmospheric Chem Phys 12:7797–7808. https://doi.org/10.5194/acp-12-7797-2012
25. Humphreys WJ (1913) Volcanic dust and other factors in the production of climatic changes, and their possible relation to ice ages. J Frankl Inst 176:131–160. https://doi.org/10.1016/S0016-0032(13)91294-1
26. Karpechko AY, Gillett NP, Dall'Amico M, Gray LJ (2010) Southern Hemisphere atmospheric circulation response to the El Chichón and Pinatubo eruptions in coupled climate models. Q J R Meteorol Soc 136:1813–1822. https://doi.org/10.1002/qj.683
27. Ke F, Hui L (2013) Evaluation of Atmospheric Circulation in the Southern Hemisphere in 20CRv2. Atmospheric Ocean Sci Lett 6:337–342. https://doi.org/10.1080/16742834.2013.11447104
28. Khodri M, Izumo T, Vialard J, et al (2017) Tropical explosive volcanic eruptions can trigger El Niño by cooling tropical Africa. Nat Commun 8:. https://doi.org/10.1038/s41467-017-00755-6
29. Kidston J, Scaife AA, Hardiman SC, et al (2015) Stratospheric influence on tropospheric jet streams, storm tracks and surface weather. Nat Geosci 8:433–440. https://doi.org/10.1038/ngeo2424
30. Krishnamohan K-PS-P, Bala G, Cao L, et al (2019) Climate system response to stratospheric sulfate aerosols: sensitivity to altitude of aerosol layer. Earth Syst Dyn 10:885–900. https://doi.org/10.5194/esd-10-885-2019

31. Langmann B (2014) On the Role of Climate Forcing by Volcanic Sulphate and Volcanic Ash. Adv Meteorol 2014:17
32. Lehner F, Schurer AP, Hegerl GC, et al (2016) The importance of ENSO phase during volcanic eruptions for detection and attribution. Geophys Res Lett 2851–2858. https://doi.org/10.1002/2016GL067935
33. Lough JM, Fritts HC (1987) An assessment of the possible effects of volcanic eruptions on North American climate using tree-ring data, 1602 to 1900 A.D. Clim Change 10:219–239. https://doi.org/10.1007/BF00143903
34. Man W, Zhou T, Jungclaus JH (2014) Effects of large volcanic eruptions on global summer climate and East Asian Monsoon changes during the Last Millennium: analysis of MPI-ESM simulations. J Clim 27:7394–7409. https://doi.org/10.1175/JCLI-D-13-00739.1
35. Marotzke J, Forster PM (2015) Forcing, feedback and internal variability in global temperature trends. Nature 517:565–570. https://doi.org/10.1038/nature14117
36. Mass CF, Portman DA (1989) Major volcanic eruptions and climate: a critical evaluation. J Clim 2:566–593. https://doi.org/10.1175/1520-0442(1989)002<0566:MVEACA>2.0.CO;2
37. McGraw MC, Barnes EA, Deser C (2016) Reconciling the observed and modeled Southern Hemisphere circulation response to volcanic eruptions: Reconciling SH Response to Volcanoes. Geophys Res Lett 43:7259–7266. https://doi.org/10.1002/2016GL069835
38. Ménégoz M, Bilbao R, Bellprat O, et al (2018) Forecasting the climate response to volcanic eruptions: prediction skill related to stratospheric aerosol forcing. Environ Res Lett 13:064022. https://doi.org/10.1088/1748-9326/aac4db
39. Neely III RR, Schmidt A (2016) VolcanEESM: Global volcanic sulphur dioxide (SO2) emissions database from 1850 to present
40. Neukom R, Barboza LA, Erb MP, et al (2019) Consistent multidecadal variability in global temperature reconstructions and simulations over the Common Era. Nat Geosci. https://doi.org/10.1038/s41561-019-0400-0
41. Oman L, Robock A, Stenchikov G, et al (2005) Climatic response to high-latitude volcanic eruptions. J Geophys Res Atmospheres 110:D13103. https://doi.org/10.1029/2004JD005487
42. Perlwitz J, Graf H-F (1995) The statistical connection between tropospheric and stratospheric circulation of the northern hemisphere in winter. J Clim 8:2281–2295
43. Picas J, Grab S (2020) Potential impacts of major nineteenth century volcanic eruptions on temperature over Cape Town, South Africa: 1834–1899. Clim Change. https://doi.org/10.1007/s10584-020-02678-6
44. Predybaylo E, Stenchikov GL, Wittenberg AT, Zeng F (2017) Impacts of a Pinatubo-size volcanic eruption on ENSO. J Geophys Res Atmospheres 122:925–947. https://doi.org/10.1002/2016JD025796
45. Raible CC, Brönnimann S, Auchmann R, et al (2016) Tambora 1815 as a test case for high impact volcanic eruptions: Earth system effects. Wiley Interdiscip Rev Clim Change 7:569–589.

https://doi.org/10.1002/wcc.407

46. Rao MP, Cook BI, Cook ER, et al (2017) European and Mediterranean hydroclimate responses to tropical volcanic forcing over the last millennium. Geophys Res Lett 44:5104–5112. https://doi.org/10.1002/2017GL073057
47. Robock A (2000) Volcanic eruptions and climate. Rev Geophys 38:191–219. https://doi.org/10.1029/1998RG000054
48. Robock A, Adams T, Moore M, et al (2007) Southern Hemisphere atmospheric circulation effects of the 1991 Mount Pinatubo eruption. Geophys Res Lett 34:L23710. https://doi.org/10.1029/2007GL031403
49. Robock A, Mao J (1995) The volcanic signal in surface temperature observations. J Clim 8:1086–1103. https://doi.org/10.1175/1520-0442(1995)008<1086:TVSIST>2.0.CO;2
50. Santer BD, Painter JF, Bonfils C, et al (2013) Human and natural influences on the changing thermal structure of the atmosphere. Proc Natl Acad Sci 110:17235–17240. https://doi.org/10.1073/pnas.1305332110
51. Sato M, Hansen JE, McCormick MP, Pollack JB (1993) Stratospheric aerosol optical depths, 1850–1990. J Geophys Res 98:22987. https://doi.org/10.1029/93JD02553
52. Shulmeister J, Goodwin I, Renwick J, et al (2004) The Southern Hemisphere westerlies in the Australasian sector over the last glacial cycle: a synthesis. Quat Int 118–119:23–53. https://doi.org/10.1016/S1040-6182(03)00129-0
53. Smith RK, Ryan BF, Troup AJ, Wilson KJ (1982) Cold Fronts Research: The Australian Summertime "Cool Change." Bull Am Meteorol Soc 63:1028–1028. https://doi.org/10.1175/1520-0477(1982)063<1028:CFRTAS>2.0.CO;2
54. Stenchikov G, Kirchner I, Robock A, et al (1998) Radiative forcing from the 1991 Mount Pinatubo volcanic eruption. J Geophys Res 103:13837–13857
55. Stevenson S, Fasullo JT, Otto-Bliesner BL, et al (2017) Role of eruption season in reconciling model and proxy responses to tropical volcanism. Proc Natl Acad Sci 114:1822–1826. https://doi.org/10.1073/pnas.1612505114
56. Stoffel M, Khodri M, Corona C, et al (2015) Estimates of volcanic-induced cooling in the Northern Hemisphere over the past 1,500 years. Nat Geosci 8:784–788. https://doi.org/10.1038/ngeo2526
57. Sun W, Wang B, Liu J, et al (2019) How northern high-latitude volcanic eruptions in different seasons affect ENSO. J Clim 32:3245–3262. https://doi.org/10.1175/JCLI-D-18-0290.1
58. Taylor KE, Stouffer RJ, Meehl GA (2012) An overview of CMIP5 and the experiment design. Bull Am Meteorol Soc 93:485–498. https://doi.org/10.1175/BAMS-D-11-00094.1
59. Timmreck C (2018) Climatic effects of large volcanic eruptions. Habilitation Thesis, Universität Hamburg
60. Tyson PD, Tyson PD, Preston-Whyte RA (2000) The Weather and Climate of Southern Africa. Oxford University Press

61. Vera CS, Vigliarolo PK (2000) A Diagnostic Study of Cold-Air Outbreaks over South America. Mon Weather Rev 128:3–24. https://doi.org/10.1175/1520-0493(2000)128<0003:ADSOCA>2.0.CO;2
62. Xia L, von Storch H, Feser F, Wu J (2015) A study of quasi-millennial extratropical winter cyclone activity over the Southern Hemisphere. Clim Dyn 47:2121–2138. https://doi.org/10.1007/s00382-015-2954-x
63. Young PJ, Thompson DWJ, Rosenlof KH, et al (2011) The Seasonal Cycle and Interannual Variability in Stratospheric Temperatures and Links to the Brewer–Dobson Circulation: An Analysis of MSU and SSU Data. J Clim 24:6243–6258. https://doi.org/10.1175/JCLI-D-10-05028.1
64. Zambri B, LeGrande AN, Robock A, Slawinska J (2017) Northern Hemisphere winter warming and summer monsoon reduction after volcanic eruptions over the last millennium. J Geophys Res Atmospheres 122:7971–7989. https://doi.org/10.1002/2017JD026728
65. Zambri B, Robock A (2016) Winter warming and summer monsoon reduction after volcanic eruptions in Coupled Model Intercomparison Project 5 (CMIP5) simulations. Geophys Res Lett 43:10,920-10,928. https://doi.org/10.1002/2016GL070460
66. Zanchettin D, Timmreck C, Graf H-F, et al (2012) Bi-decadal variability excited in the coupled ocean–atmosphere system by strong tropical volcanic eruptions. Clim Dyn 39:419–444. https://doi.org/10.1007/s00382-011-1167-1
67. Zhang D, Blender R, Fraedrich K (2013a) Volcanoes and ENSO in millennium simulations: global impacts and regional reconstructions in East Asia. Theor Appl Climatol 111:437–454. https://doi.org/10.1007/s00704-012-0670-6
68. Zhang Q, Körnich H, Holmgren K (2013b) How well do reanalyses represent the southern African precipitation? Clim Dyn 40:951–962. https://doi.org/10.1007/s00382-012-1423-z
69. Zuo M, Man W, Zhou T, Guo Z (2018) Different impacts of Northern, Tropical, and Southern Volcanic Eruptions on the Tropical Pacific SST in the Last Millennium. J Clim 31:6729–6744. https://doi.org/10.1175/JCLI-D-17-0571.1

Tables

Due to technical limitations, table 1-2 is only available as a download in the Supplemental Files section.

Figures

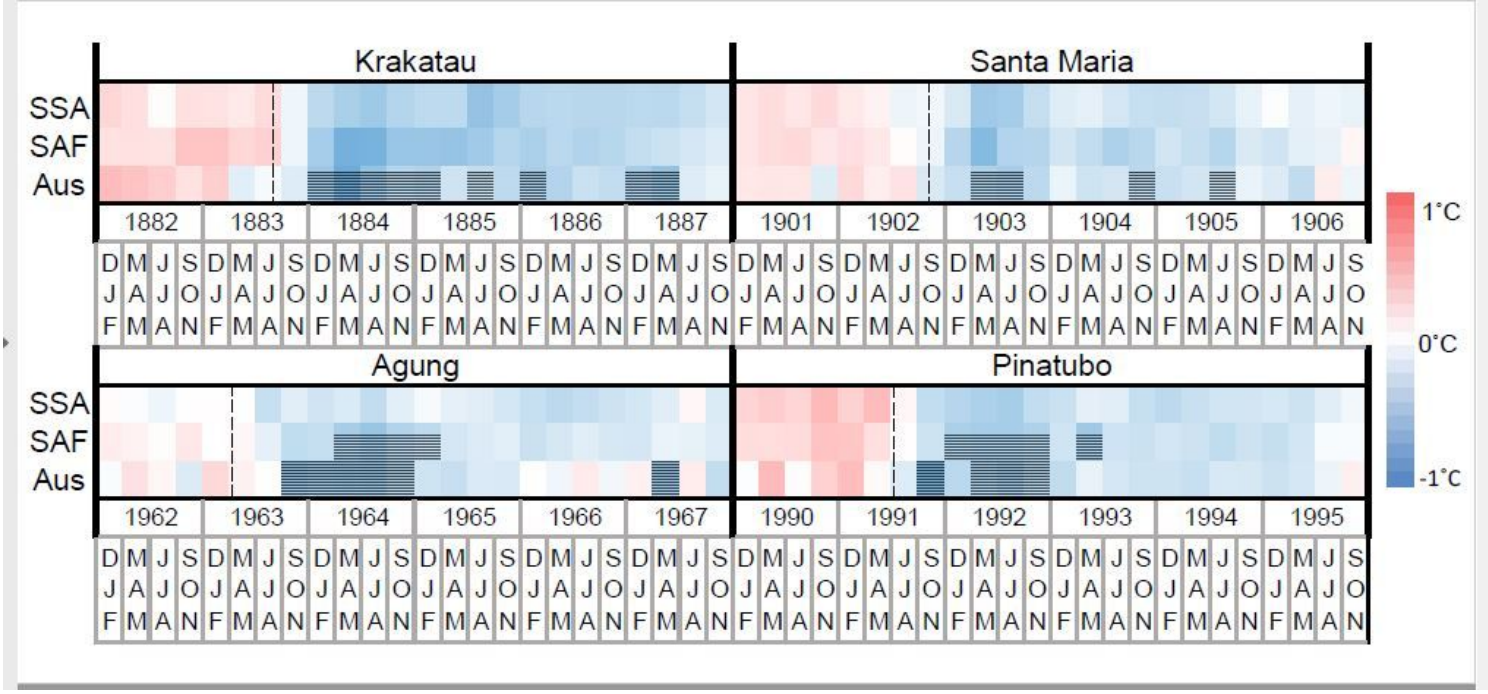

Figure 1

CMIP5 seasonal temperature anomalies for each continent in the SH (southern South America (SSA); southern Africa (SAF) and Australia (Aus)), over the period for each of the four eruptions (Krakatau, Santa Maria, Agung, Pinatubo), starting two years before the eruption and ending three years after the event. The vertical dashed lines represent the eruption event. Blocks with hashed lines represent significant anomalies.

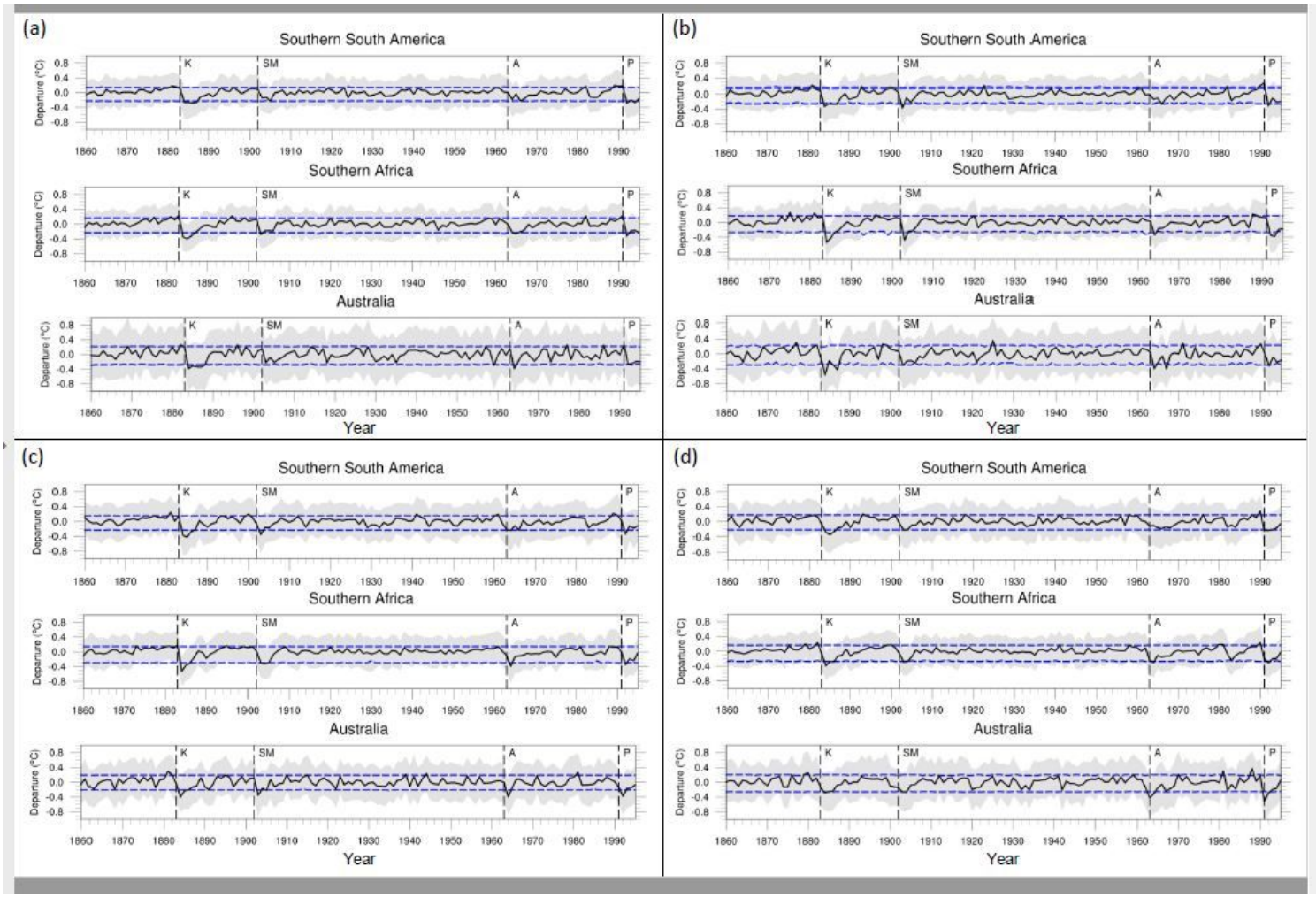

Figure 2

CMIP5 seasonal near-surface temperature anomalies for the continents of southern South America, southern Africa and Australia for the seasons of (a) austral summer (DJF), (b) autumn (MAM), (c) winter (JJA) and (d) spring (SON). Gray shading = 25th and 75th percentile ensemble spread, blue dashed lines= statistical significance (90% confidence interval), dashed vertical lines = eruption events of (K) Krakatau, (SM) Santa Maria, (A) Agung, and (P) Pinatubo.

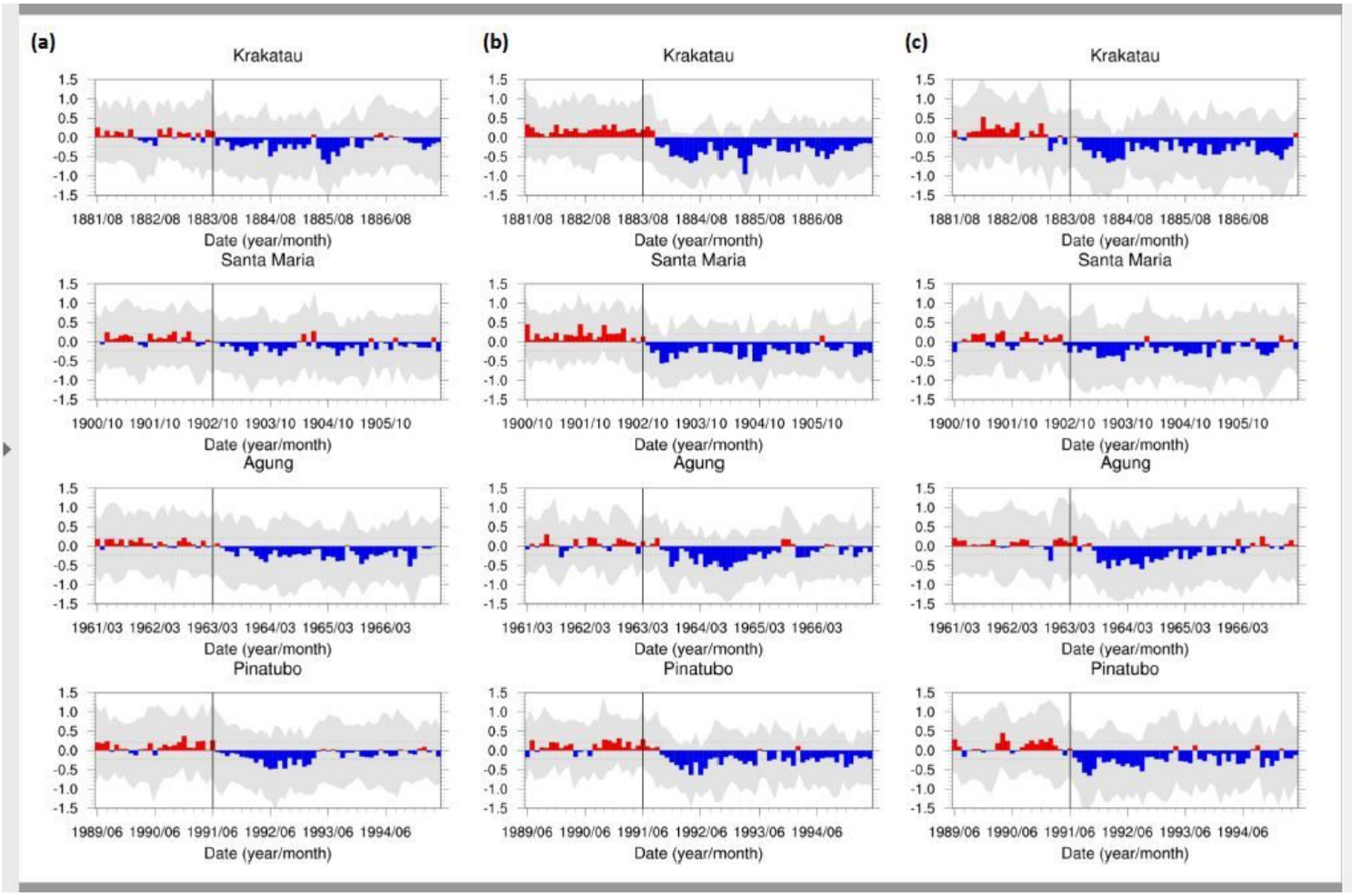

Figure 3

CMIP5 monthly near-surface temperature anomalies for the continents of (a) southern South America, (b) southern Africa and (c) Australia for each of the four major eruptions. Gray shading = ensemble spread between 25th and 75th percentiles.

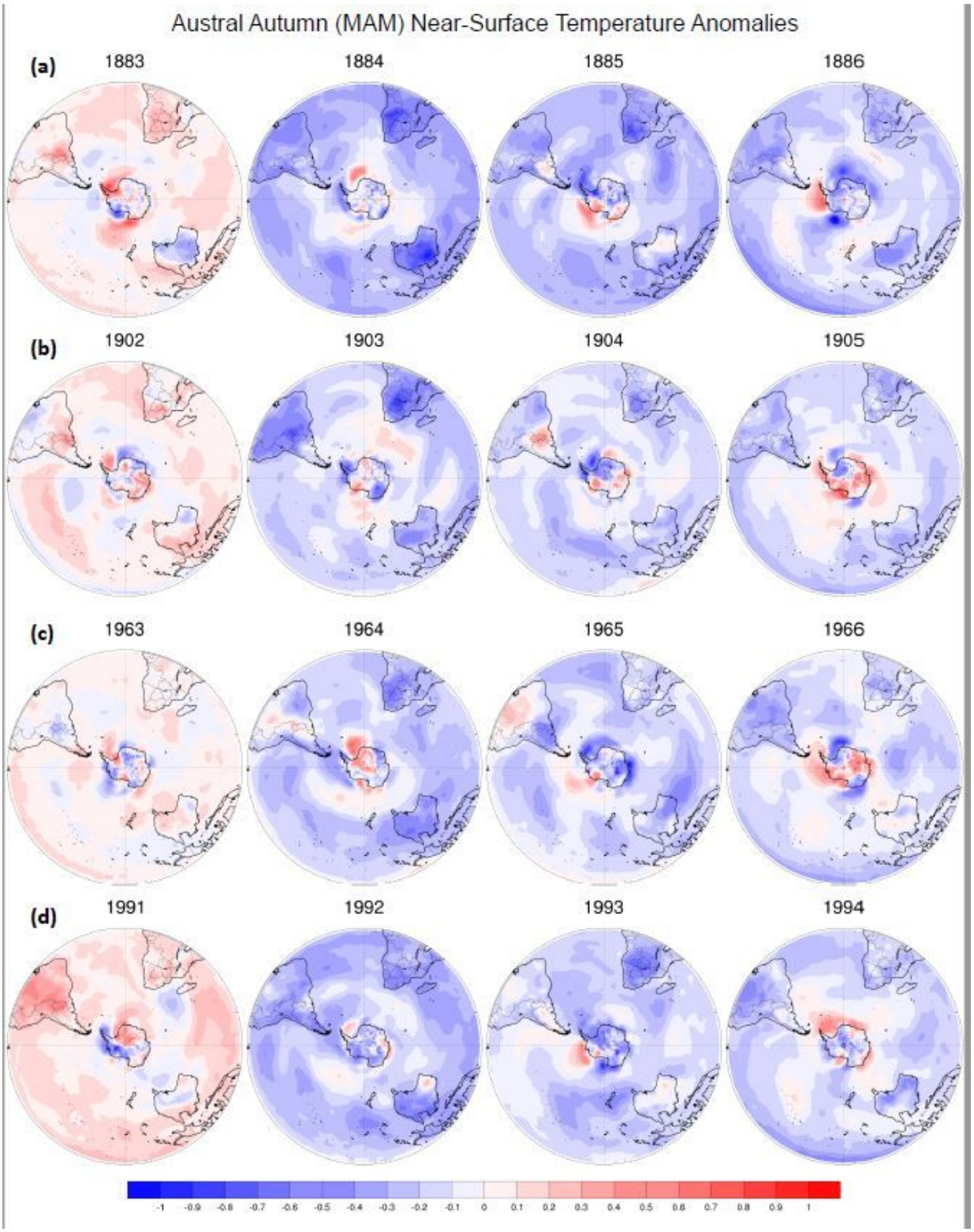

Figure 4

CMIP5 spatial maps of austral autumn temperature anomalies over the SH for the eruptions of (a) Krakatau, (b) Santa Maria, (c) Agung and (d) Pinatubo. The same figures for summer, winter and spring can be found in the Online Resource 1 (Fig. S1, Fig. S2, Fig. S3). Note: The designations employed and the presentation of the material on this map do not imply the expression of any opinion whatsoever on the part of Research Square concerning the legal status of any country, territory, city or area or of its

authorities, or concerning the delimitation of its frontiers or boundaries. This map has been provided by the authors.

Supplementary Files

This is a list of supplementary files associated with this preprint. Click to download.

- SupplementaryMaterial.docx
- Table1.xlsx
- Table2.xlsx